Complexity on dwarf galaxy scales

Breddels, Maarten; Helmi, Amina

Published in:
The Astrophysical Journal

DOI:
10.1088/2041-8205/791/1/L3

The Astrophysical Journal Letters, 791:L3 (4pp), 2014 August 10 doi:10.1088/2041-8205/791/1/L3

COMPLEXITY ON DWARF GALAXY SCALES: A BIMODAL DISTRIBUTION FUNCTION IN SCULPTOR

Maarten A. Breddels and Amina Helmi
Kapteyn Astronomical Institute, University of Groningen, P.O. Box 800, 9700-AV Groningen, The Netherlands; breddels@astro.rug.nl
Received 2014 April 23; accepted 2014 June 30; published 2014 July 22

ABSTRACT

In our previous work, we presented Schwarzschild models of the Sculptor dwarf spheroidal galaxy demonstrating that this system could be embedded in dark matter halos that are either cusped or cored. Here, we show that the non-parametric distribution function recovered through Schwarzschild's method is bimodal in energy and angular momentum space for all of the best-fitting mass models explored. We demonstrate that this bimodality is directly related to the two components known to be present in Sculptor through stellar population analysis, although our method is purely dynamical in nature and does not use this prior information. It therefore constitutes independent confirmation of the existence of two physically distinct dynamical components in Sculptor and suggests a rather complex assembly history for this dwarf galaxy.

Key words: galaxies: dwarf – galaxies: kinematics and dynamics

Online-only material: color figures

1. INTRODUCTION

Sculptor (Scl) was the first dwarf spheroidal (dSph) galaxy discovered (Shapley 1938), and it may be considered an archetype of the class of dSph galaxies as it is a rather featureless system (compared to, e.g., Fornax; de Boer et al. 2011). Nonetheless, Scl has proven to be more complex than originally thought. Photometric surveys starting from Da Costa (1984) and later by Light (1988), Hurley-Keller et al. (1999), and Majewski et al. (1999) have revealed that its horizontal branch morphology changes with radius. More recently, due to large spectroscopic surveys, it has been possible to relate the differences in the spatial distribution of the blue and red horizontal branches (BHB/RHB) to differences in the chemical composition and kinematics of its stars (Tolstoy et al. 2004), as well as to age gradients (de Boer et al. 2011).

The picture that has emerged from this body of work is that Scl has two populations or components. The first population is centrally concentrated, metal-rich, younger, is represented in RHB stars, and has colder kinematics, with a decreasing line-of-sight velocity dispersion with distance from the center. The second population is less concentrated, metal-poor, older, is prominent in BHB stars, has hotter kinematics, and a more constant velocity dispersion profile. It was not clear until now whether this could simply be due to a population gradient.

dSph galaxies have been the target of many kinematic surveys in the past decade because of their very high dynamical mass-to-light ratios. The aim of these studies has been to provide constraints on the nature and distribution of dark matter; however, no firm conclusions have yet been drawn. This is because of limitations in the data (access to only line-of-sight velocities) and also in the models. For example, the most widely used modeling technique is based on the Jeans equations and requires making assumptions about the orbital structure of the system (see, e.g., Walker et al. 2009b), although recent work by Richardson & Fairbairn (2013, 2014) using higher moments and virial equations seems to be able to circumvent this degeneracy. A more powerful approach is to use orbit-based dynamical modeling, also known as Schwarzschild's method. Breddels et al. (2013) have shown that the data on Scl does not constrain the inner slope of its dark matter density profile very strongly, and that neither cored nor cuspy (of the Navarro–Frenk–White (NFW)-type; Navarro et al. 1996) profiles are favored.

On the other hand, it has been argued that the multiple components present in Scl should be used to model this system dynamically and that this ought to lead to much tighter constraints. This is because these components are hosted by the same underlying potential and their presence would effectively reduce the available parameter space of plausible dynamical models (Battaglia et al. 2008). Several studies have attempted this using, e.g., the virial equations (Agnello & Evans 2012) or constraints based on Jeans modeling (Walker & Peñarrubia 2011; Amorisco & Evans 2012b), and concluded that NFW-like profiles are strongly disfavored. All of these works (with the exception of Walker & Peñarrubia 2011) have assumed that the two populations are split in the same way in photometry and kinematics/chemistry, although this is not guaranteed a priori, as the kinematics (and split in metallicity) are obtained from the red giant branch while the photometry is fit for the BHB and RHB stars independently. Perhaps more importantly, all of these models based on a single estimate of the mass at a given radius (e.g., either through Jeans or through the virial equations) have assumed the components to follow the same functional form of the light distribution (with different characteristic parameters). As we will show below, this is not necessarily a valid assumption.

In this Letter, we analyze the phase-space structure of the best-fitting Schwarzschild dynamical models of Scl from Breddels & Helmi (2013) and Breddels (2013). Our spherical orbit-based dynamical models are non-parametric in the distribution function (e.g., no assumptions are made concerning the anisotropy) and provide good fits to the global kinematics and light distribution of Scl. The dark matter distribution follows specific parametric profiles (see Jardel et al. 2012), which all produce very similar mass distributions in a finite region around the half-light radius of Scl. As we will show below, the orbit weights (which correspond to the distribution function of the galaxy) show a bimodal distribution for all of the best-fit models of Scl, even though this is not a priori assumed.

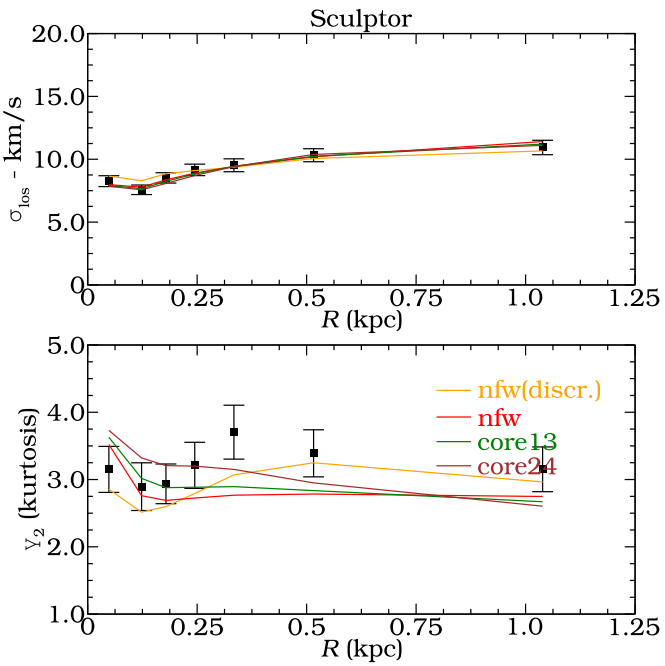

Figure 1. Velocity dispersion (top panel) and kurtosis (lower panel) for the best-fitting models for different dark matter profiles, namely, Navarro–Frenk–White (NFW; based on moments or discrete modeling of the data) and two cored profiles with $\rho(r) \propto 1/(r + r_c)^3$ (core13) and $\rho(r) \propto 1/(r^2 + r_c^2)^2$ (core24).

(A color version of this figure is available in the online journal.)

2. DISTRIBUTION FUNCTIONS OBTAINED VIA SCHWARZSCHILD MODELS

Our orbit-based dynamical models are described extensively in Breddels et al. (2013). This method essentially consists of finding a linear combination of orbits (integrated in a given gravitational potential) which allows fitting the kinematic data and light distribution of the system. By varying the characteristic parameters of the gravitational potential (e.g., mass and scale radius), best fits are found, while the weights of the orbits effectively provide the distribution function non-parametrically.

Figure 1 shows how well the best-fit models for various dark matter profiles explored in Breddels & Helmi (2013) and from the discrete modeling approach by Breddels (2013) reproduce the velocity dispersion and kurtosis profiles. As can be seen from this figure, the resulting fits are nearly indistinguishable from one another.

Figure 2 shows the orbit weights that define the distribution functions of the best-fit models explored. For example, the best-fit NFW model found in Breddels (2013), obtained using discrete fitting, is given in the upper left panel. The associated distribution function appears to be bimodal as it has two distinct components: one at low angular momentum (near energy index 8, angular momentum index 2), and a second one at higher angular momentum (near energy index 7, angular momentum index 6). This bimodality is also present in the distribution functions of the remaining best-fitting models from Breddels & Helmi (2013), whether cored or cusped. Although the exact location of the lower angular momentum component varies slightly, it is reassuring that the bimodality is found using both the discrete and the traditional Schwarzschild methods and also for different dark matter profiles. This demonstrates the power of using non-parametric Schwarzschild methods.

To obtain further insights into the nature of these two components, we use a watershed algorithm. We first locate the local

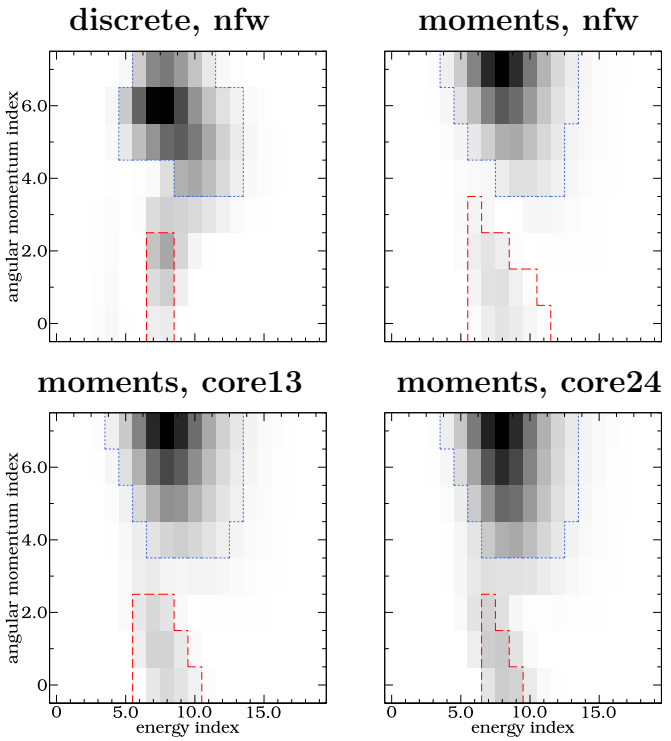

Figure 2. Orbit weights for the best-fit models for different dark matter halo profiles: discrete NFW (Breddels 2013, top left), moment-based NFW (top right), and cored (bottom) models from Breddels & Helmi (2013). The red dashed and blue solid contours indicate the two components found by the watershed method.

(A color version of this figure is available in the online journal.)

maxima in the image, which serve to identify the two different components. Starting from the pixel with the maxima, we follow the landscape downward, i.e., we find those neighboring pixels that have a lower value. These are associated with either of the components until no more such pixels are found. At this point, we exclude pixels that could be simultaneously associated with both components. In Figure 2, we indicate the pixels associated with each of the two components by showing the contours that correspond to 5% of the maximum orbital-weight for each component. We then construct two distribution functions by selecting the pixels identified by the algorithm as just described. We now refer to the higher and lower angular momentum components as the blue and red components, respectively.

3. THE NATURE OF THE BIMODALITY

From the distribution function, we can derive the line-of-sight velocity as well as the surface brightness profiles for each component. This is useful in order to understand the link to the cold/hotter kinematic or RHB/BHB populations known to exist in Scl. In Figure 3, we show the line-of-sight velocity dispersion profiles for the two components separately, where each panel corresponds to the best-fit models shown in Figure 2. The red component shows an increasing velocity dispersion toward the center and falls off rapidly with radius, while the blue component has a flatter profile.

These trends are quite similar to the velocity dispersion profiles shown at the bottom of the figure for the metal-rich (MR) and metal-poor (MP) components defined as those stars with [Fe/H] > -1.5 dex (red) and [Fe/H] < -1.7 dex (blue) in Battaglia et al. (2008). In this figure, we have also added

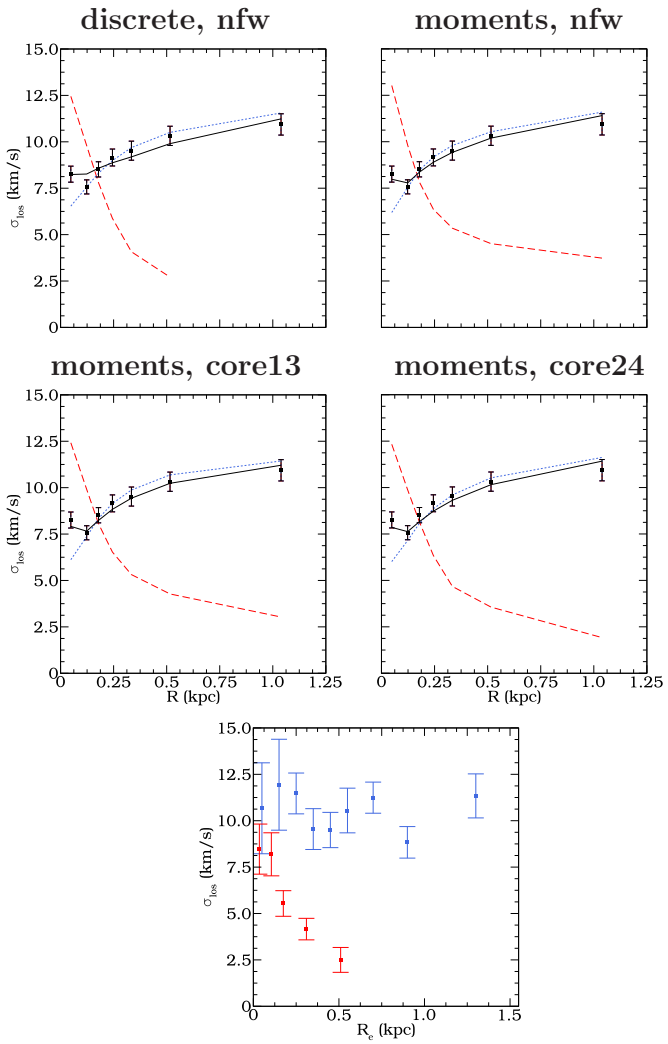

Figure 3. Black points with error bars show the velocity dispersion profile for Scl. The top four panels show the σ_{los} for each of our best-fitting models, separately for the low angular momentum (dashed red) and high angular momentum components (dotted blue) as identified in Figure 2. The bottom panel shows the velocity dispersion profiles as function of elliptical radii for the metal-rich and metal-poor populations in Sculptor, using data from Battaglia et al. (2008) and also from Walker et al. (2009a) for the outermost bins (see the text for more details).

(A color version of this figure is available in the online journal.)

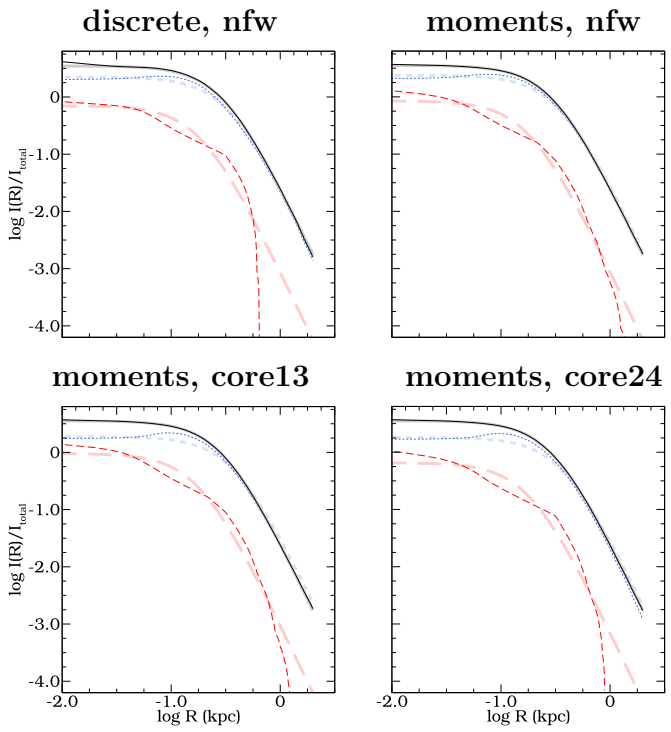

Figure 4. Density of the projected light distribution for the two components, similar to Figure 3. The solid black graph indicates the total light distribution. Thicker and semi-transparent lines indicate the best-fitting Plummer profile.

(A color version of this figure is available in the online journal.)

Table 1
Plummer Scale Radii b for the Red (Low Angular Momentum) and Blue (High Angular Momentum) Components, and for the Total Light Distribution

	b_{red}	b_{blue}	b_{total}	f_{red}	f_{int}	f_{blue}
NFW(discrete)	0.19	0.34	0.3	0.080	0.109	0.812
NFW	0.18	0.35	0.3	0.088	0.020	0.892
Core13	0.18	0.38	0.3	0.097	0.045	0.858
Core24	0.18	0.37	0.3	0.069	0.129	0.802

Note. The last three columns give the mass fractions associated with the red, blue, and intermediate components.

the data from Walker et al. (2009a) in the four outermost bins for a fairer comparison to the data shown in the top panels and used for the Schwarzschild models. Note that the sharp [Fe/H] cuts used in this panel to define the two populations do not guarantee the absence of cross-contamination, especially in the inner regions where the populations spatially overlap. In fact, any misassignment in the center will tend to lower the dispersion of the MR population, while increasing that of the MP, as perhaps these comparisons suggest.

In Figure 4, we show the projected light distribution for each of the two identified components (in red and blue for low and high angular momenta, respectively), as well as for the full system (in black). This figure clearly shows that the red component is more centrally concentrated than the blue component for all models. This can be quantified further by fitting a Plummer profile to each component separately. The results are given in Table 1. Note, however, that the Plummer functional form does not fit well the light distribution of the more concentrated, lower angular momentum component (which is somewhat better fit with an exponential). Typically, the ratio of the Plummer scale radii is $b_{red}/b_{blue} \sim 0.5$, which is comparable to the ratio determined by fitting the Plummer profiles to the RHB and BHB populations separately, which is $r = 0.6$ according to Battaglia (2007). However, recall that the photometric and even the spectroscopic decomposition do not necessarily correspond to the dynamical components found by our method. Nonetheless, the similarities are striking.

In terms of the velocity anisotropies of the two detected components, we find the low angular momentum component to be radially anisotropic in all cases considered. On the other hand, the high angular momentum component is tangentially biased over most radii in all models, but it shows larger model to model variations. These reflect the differences in the detailed form of the distribution function which can be seen in Figure 2.

In the above analysis, parts of the distribution function were not assigned to either of the two components (e.g., typically in the region in between). None of the conclusions we have reached so far are very sensitive to whether this intermediate mass is assigned to the red or the blue components. We have

found by assigning this intermediate mass to the blue or red components, respectively, that the surface brightness profiles become smoother (i.e., less bumpy), but that the changes to the velocity dispersion profiles are very small ($<1\,\mathrm{km\,s^{-1}}$). In particular, the blue and red components remain clearly kinematically distinct in the central regions. The fractional masses for the intermediate component for each model can be found in the right columns of Table 1.

4. DISCUSSION AND CONCLUSIONS

We have shown that the distribution function of Scl for several best-fitting mass models is bimodal in energy and angular momentum space. The two components may be split into low and high angular momentum parts using the watershed method. The properties of the low and high angular momentum components are similar to the metal-rich and metal-poor components, respectively, known to be present in this galaxy, in terms of their velocity dispersion profile and their light distribution (Battaglia et al. 2008).

This result is quite remarkable since we have not assumed at any point the existence of multiple components in the Scl dwarf. This therefore suggests that the metal-rich and metal-poor stars are indeed dynamically distinct, and that Scl is not simply a system with a radial gradient in stellar populations. This finding highlights the full power of the Schwarzschild's dynamical approach, and would not have been possible if we had taken a parametric approach to model the distribution function.

The fact that our models naturally recover the bimodality present in Scl for all dark matter profiles explored, and even for the NFW form, would seem to be at odds with the results of Agnello & Evans (2012) and Walker & Peñarrubia (2011). In these works, Scl was modeled as a two-component system with light distributions that followed similar profiles. The use of the virial equations or the robust estimator of the mass at the half-light radii of each component was used to argue that NFW profiles could be ruled out with high significance. Our modeling, however, shows this is not the case and why it is not. The assumption of similar light profiles appears to be crucial to reach those conclusions, and would seem to introduce a systematic bias that none of these works have taken into account. In the resulting non-parametric dynamical models we have obtained, the light distribution for the two components is quite different and cannot be parameterized well by Plummer profiles, as shown by Figure 4. M. G. Walker (2014, private communication) repeated the analysis of Walker & Peñarrubia (2011), but now allowing the metal-rich profile to follow an exponential form. While still excluding a cusp with $p > 98.4\%$ instead of $p > 99.8\%$, it demonstrates the bias caused by the assumed parametric form of the light profiles.

It is natural to wonder whether other dwarfs also exhibit multiple dynamical components. Fornax would be a natural candidate but its complex light distribution (e.g., the presence of shells, non-axisymmetries in the center; Battaglia et al. 2006) and the hints of misaligned kinematics (see, e.g., Amorisco & Evans 2012a) require the use of a more general (non-spherical) Schwarzschild modeling approach. On the other hand, it would be desirable to have larger data sets, e.g., for Carina and Sextans, to be confident in the robustness of the analyses. More generally, an interesting challenge will be to understand how such complex systems can form on the smallest galaxy scale, i.e., on the scale of the dSphs.

A.H. and M.B. are grateful to NOVA for financial support. AH acknowledges financial support the European Research Council under ERC-Starting Grant GALACTICA-240271.

REFERENCES

Agnello, A., & Evans, N. W. 2012, ApJL, 754, L39
Amorisco, N. C., & Evans, N. W. 2012a, ApJL, 756, L2
Amorisco, N. C., & Evans, N. W. 2012b, MNRAS, 419, 184
Battaglia, G. 2007, PhD thesis, Kapteyn Astronomical Institute, Univ. Groningen
Battaglia, G., Helmi, A., Tolstoy, E., et al. 2008, ApJL, 681, L13
Battaglia, G., Tolstoy, E., Helmi, A., et al. 2006, A&A, 459, 423
Breddels, M. 2013, PhD thesis, Kapteyn Astronomical Institute, Univ. Groningen
Breddels, M. A., & Helmi, A. 2013, arXiv:1304.2976
Breddels, M. A., Helmi, A., van den Bosch, R. C. E., van de Ven, G., & Battaglia, G. 2013, MNRAS, 433, 3173
Da Costa, G. S. 1984, ApJ, 285, 483
de Boer, T. J. L., Tolstoy, E., Saha, A., et al. 2011, A&A, 528, A119
Hurley-Keller, D., Mateo, M., & Grebel, E. K. 1999, ApJL, 523, L25
Jardel, J. R., Gebhardt, K., Fabricius, M., Drory, N., & Williams, M. J. 2012, arXiv:1211.5376
Light, R. M. 1988, PhD thesis, Yale Univ.
Majewski, S. R., Siegel, M. H., Patterson, R. J., & Rood, R. T. 1999, ApJL, 520, L33
Navarro, J. F., Frenk, C. S., & White, S. D. M. 1996, ApJ, 462, 563
Richardson, T., & Fairbairn, M. 2013, MNRAS, 432, 3361
Richardson, T., & Fairbairn, M. 2014, MNRAS, in press (arXiv:1207.1709)
Shapley, H. 1938, Natur, 142, 715
Tolstoy, E., Irwin, M. J., Helmi, A., et al. 2004, ApJL, 617, L119
Walker, M. G., Mateo, M., & Olszewski, E. W. 2009a, AJ, 137, 3100
Walker, M. G., Mateo, M., Olszewski, E. W., et al. 2009b, ApJ, 704, 1274
Walker, M. G., & Peñarrubia, J. 2011, ApJ, 742, 20